

# Evolution of deformations in medium-mass nuclei

H. Sagawa, X. R. Zhou <sup>\*</sup> and X. Z. Zhang <sup>†</sup>

*Center for Mathematical Sciences,  
University of Aizu  
Aizu-Wakamatsu,  
Fukushima 965-8560, Japan  
E-mail: sagawa@u-aizu.ac.jp*

## Abstract

Evolution of quadrupole deformations in *sd* and *pf* shell nuclei with mass  $A=18\sim 56$  is studied by using deformed Skyrme Hartree-Fock (HF) model with pairing correlations. We point out that the quadrupole deformations of the nuclei with the isospin  $T=0$  and  $T=1$  show strong mass number dependence as a clear manifestation of dynamical evolution of deformation in nuclear many-body systems. The competition between the deformation driving particle-vibration coupling and the closed shell structure is shown in a systematic study of the ratios between the proton and neutron deformations in nuclei with  $T=|T_z|=1$ . Calculated quadrupole and hexadecapole deformations are compared with shell model results and available experimental data. A relation between the skin thickness and the intrinsic  $Q_2$  moments is also discussed.

PACS numbers: 21.10.Ky, 21.60.Cs, 21.60.Jz, 23.20.-g

---

<sup>\*</sup> present address: Department of Physics, Xiamen University, Xiamen 361005, P. R. China

<sup>†</sup> On leave from China Institute of Atomic Energy , Beijing, China

## I. INTRODUCTION

A study of the mass number dependence of the deformations in nuclei is an interesting subject in relation to a manifestation of spontaneous symmetry breaking in quantum many-body systems. The effect of spontaneous symmetry breaking is a general phenomenon known in many fields of physics. In molecular physics, the spontaneous symmetry breaking was discovered by Jahn and Teller in 1937 [1]. The coupling to the quadrupole vibration is the main origin of the static deformation in both molecules and atomic nuclei [2]. The pairing correlation in atomic nuclei is known to stabilize the spherical symmetry. An unique feature of the evolution of deformation in atomic nuclei will appear in the competition between the deformation deriving particle-vibration coupling and the pairing correlations [3]. Top of that, the shell structure of nuclei will give rise to a variety of different shapes, i.e., prolate, oblate and triaxial shapes depending on the position of the Fermi energy between two closed shells.

Electromagnetic observables provide useful information to study structure of nuclei of both ground states and excited states. Namely, the observables such as quadrupole ( $Q_2$ ) moments and electric quadrupole (E2) transitions are expected to pin down precise information of deformations. The evolution mechanism of deformation will change the shapes of nuclei from the beginning to the end of the closed shell. Up to now, the mass number dependence of the deformations has been studied mainly in rare earth nuclei. However, it is rather difficult in rare-earth and heavy nuclei to study the deformations systematically between two closed shells due to the limitation of available nuclei for experiments. On the other hand, it is possible to access experimentally from the beginning to the end of the closed shell in *sd* and *pf* shell nuclei. Thus, the *sd* and *pf* shell nuclei might be promising candidates to discuss the dynamical evolution of deformation since several electric quadrupole transitions are already observed [4] and new data of proton-rich unstable nuclei are also available [5–7].

The main aim of this paper is to study the dynamical evolution of nuclear deformation in *sd* and *pf* shell nuclei with the isospin  $T=0$  and 1 including unstable proton-rich nuclei. To this end, we perform deformed Skyrme Hartree-Fock (HF)+BCS calculations with a density-dependent pairing interaction in nuclei of mass number  $A=(16\sim 56)$ . Firstly, the mass number dependence of proton deformation is examined in comparison with empirical values extracted from the electric quadrupole transition strength  $B(E2)$  of the  $T=0$  nuclei. The quadrupole moments of the first excited  $2^+$  states are also studied to extract the sign and the magnitude of the intrinsic quadrupole deformations. Then the ratios between calculated proton and neutron deformations of  $T=1$  nuclei are compared with shell model results and empirical values obtained from  $B(E2)$  values of mirror nuclei with  $T=1$  and  $T_z = \pm 1$ , assuming the isospin symmetry in the two nuclei. The evolution of higher multipole deformation is also an interesting subject related with the shell filling effect of the deformed potential. We will study the hexadecapole deformation by using the deformed HF wave function and compared with available empirical data.

This paper is organized as follows. The effect of the dynamical symmetry breaking on nuclear deformation is reviewed in Section IIA. Deformed HF+BCS calculations with Skyrme forces and a density dependent pairing interactions are presented in Section IIB. The calculated quadrupole moments are compared with experimental data in Section IIB and IIC. The isospin symmetry of the intrinsic  $Q_2$  moments is discussed in comparison with shell model calculations and other mean field models in Sections IIIA and IIIB. A relation between the skin thickness and  $Q$  moments is mentioned in Section IIIB. Section

IIRC is devoted to the study of hexadecapole deformations of the  $sd$ - and  $pf$ -shell nuclei calculated by the HF wave functions and compared with available experimental data. A summary is given in Section IV.

## II. DEFORMATIONS IN MEDIUM-HEAVY NUCLEI IN MEAN FIELD THEORY

### A. Spontaneous symmetry breaking and pairing correlations

The phenomenon of spontaneous symmetry breaking appears in many field of physics. As an example of the symmetry breaking, the deformation effect was observed commonly in quantum many-body systems, not only in molecules, but also atomic nuclei and atomic clusters. The spontaneous symmetry breaking was recognized also in the field theory, superconductors and condensed matter physics. Recently, it was discussed in relation to the chiral band of tri-axial nuclei [8].

Let us briefly discuss the spontaneous symmetry breaking effect to derive the nuclear deformation. The simplest example is the case of two degenerate single-particle states interacting with one collective mode denoted by the normal mode coordinate  $Q$ . The collective hamiltonian for the system can be given by the sum of the kinetic energy and the potential energy ,

$$H(Q) = -\frac{1}{2} \frac{\partial^2}{\partial Q^2} + \frac{1}{2} Q^2 - kQ \begin{pmatrix} 1 & 0 \\ 0 & -1 \end{pmatrix} \quad (1)$$

where the energy unit of this hamiltonian (1) is the eigenvalue of the normal mode. This collective hamiltonian is obtained based on the Born-Oppenheimer approximation, i.e., the decoupling between the collective and single particle motions. This hamiltonian gives the potential minima of  $E = -k^2/2$  at both side of the deformation

$$Q = \pm k \quad (k > 0) \quad (2)$$

The positive value  $+k$  gives a prolate deformation, while the negative value  $-k$  gives an oblate deformation. The pairing correlations play an important role for the structure of not only ground states but also excited states in nuclei. The interplay between the deformation driving force and the pairing correlations gives an unique feature of the symmetry breaking of atomic nuclei compared to other quantum many-body systems [3]. We will discuss the effect of pairing correlations on the deformation later in this section and also in Section IIIA.

For a harmonic oscillator potential in the limit of large quantum numbers, there is a symmetry between the prolate shape occurring at the beginning of the shell and the oblate shape at the end of the shell [9]. The HF neutron single-particle energies of  $^{30}\text{Si}$  are given in Fig. 1 as a function of the deformation parameter  $\beta_2$ . In  $sd$  shell nuclei, the strong preference for prolate deformation in the beginning of the shell can be understood from the fact that the energy of the orbit  $K^\pi=1/2^+$  from  $1d_{5/2}$  orbit (in the spherical limit) decreases more strongly as a function of deformation than do any of the orbits in a potential of oblate shape near the Fermi surface as is shown in Fig. 1. Namely the strength of the linear term in the hamiltonian (1) is the largest for the prolate side at the beginning of the shell in the HF calculations. For the harmonic oscillator potential, one would expect a preference of the oblate shape at the end of the shell due to the symmetry of the single-particle energies. However, the spin-orbit force and the  $\vec{l}^2$  term in the potential reduce the driving force for oblate deformation although the argument of the harmonic oscillator potential prefers it in

the latter half region of the closed shell. Thus, in most of nuclei, the calculated and observed deformations are very much dominated by the prolate shape [10]. However, in light nuclei like C and Ne isotopes, it was pointed out that the deformation will change in a similar way to be expected from the deformed harmonic oscillator potential since the spin-orbit force and the  $\vec{l}^2$  term are relatively small in the mean fields of these isotopes [11].

Higher multipole deformations are also associated with the spontaneous symmetry breaking of nucleus. The effect of the shell filling in deformed potentials was discussed on the higher multipole deformations in refs. [9] and [12]. We focus on the hexadecapole deformation  $Q_4$  in this paper and discuss the mass number dependence of it.

In the past, many theoretical model calculations were performed to study the masses and the deformations in *sd* and *pf* shell nuclei (See, for examples, review articles of various models in refs. [13, 14]. Ragnarsson and Sheline carried out the Nilsson Strutinsky type calculations with modified oscillator potential to discuss the deformation of nuclei in the whole nuclear periodic table [15, 16]. Moller and collaborators performed very extensive calculations with a finite-range droplet model (FRDM) in the whole mass region from  $^{16}\text{O}$  to  $^{339}\text{136}$  [17]. Various self-consistent models are also applied to study the medium mass nuclei; HF model [12, 18, 19], HF+BCS model [20], HF+Bogoliubov model [21, 22]. Tri-axial rotor model was also used to study the deformation in  $^{30}\text{S}$  [23].

## B. Mass number dependence of deformations in T=0 nuclei

We investigate the mass number dependence of deformations in *sd* and *pf* shell nuclei with the isospin T=0 and T=1. To this end, we perform deformed HF+BCS calculations with two Skyrme interactions SGII and SIII to see the interaction dependence of the results. Both interactions are commonly used in the mean field calculations and also random phase approximations for the excited states. The axial symmetry is assumed for the HF deformed potential. The pairing interaction is taken to be a density dependent pairing interaction in BCS approximation;

$$V(\mathbf{r}_1, \mathbf{r}_2) = V'_0 \left( 1 - \frac{\rho(r)}{\rho_0} \right) \delta(\mathbf{r}_1 - \mathbf{r}_2) \quad (3)$$

where  $\rho(r)$  is the HF density at  $\mathbf{r} = (\mathbf{r}_1 + \mathbf{r}_2)/2$  and  $\rho_0$  is chosen to be  $0.16 \text{ fm}^{-3}$ . The pairing strength is taken to be  $V'_0 = -410 \text{ MeV} \cdot \text{fm}^3$  for both neutrons and protons [24]. A smooth energy cut-off is employed in the BCS calculations [25]. We study in this section quadrupole moments  $Q_2$  using the constrained deformed HF wave functions. The constraint is imposed on the axial mass quadrupole moment operator  $\hat{Q}_{20}$ . The intrinsic proton  $Q_{2p}$  and neutron  $Q_{2n}$  moments are calculated by using HF wave function  $|K\rangle$ ,

$$Q_{2p} = \langle K | \int \hat{\rho}_p(x, y, z)(2z^2 - x^2 - y^2) d\mathbf{r} | K \rangle \quad (4)$$

$$Q_{2n} = \langle K | \int \hat{\rho}_n(x, y, z)(2z^2 - x^2 - y^2) d\mathbf{r} | K \rangle \quad (5)$$

where  $\hat{\rho}_p$  and  $\hat{\rho}_n$  are the proton and the neutron density operators. The intrinsic proton hexadecapole  $Q_{4p}$  and neutron hexadecapole  $Q_{4n}$  moments are also calculated by using HF

wave function  $|K\rangle$ ,

$$Q_{4p} = \langle K | \int \hat{\rho}_p(x, y, z)(2z^4 - 6z^2(x^2 + y^2) + \frac{3}{4}(x^2 + y^2)^2) d\mathbf{r} | K \rangle \quad (6)$$

$$Q_{4n} = \langle K | \int \hat{\rho}_n(x, y, z)(2z^4 - 6z^2(x^2 + y^2) + \frac{3}{4}(x^2 + y^2)^2) d\mathbf{r} | K \rangle \quad (7)$$

The electric multipole transition strength  $B(E\lambda)$  in the laboratory system can be expressed as

$$B(E\lambda; KI_i \rightarrow KI_f) = \frac{2\lambda + 1}{16\pi} (eQ_{\lambda p})^2 \langle I_i K \lambda 0 | I_f K \rangle^2 \quad (8)$$

with the intrinsic  $Q_{\lambda p}$  moment. Furthermore, the quadrupole moment of the excited  $2^+$  state  $Q_2(2^+)$  can be calculated by using the intrinsic quadrupole moment  $Q_{2p}$ ;

$$Q_2(2^+) = -\frac{2}{7} Q_{2p}. \quad (9)$$

The magnitude of intrinsic  $Q_{\lambda p}$  moments can be extracted experimentally from observed  $B(E\lambda)$  values by using Eq. (8). The observed  $Q_2(2^+)$  moment will be useful to extract not only the magnitude but also the sign of the intrinsic  $Q_{2p}$  moment from Eq. (9).

In Fig. 2, the calculated HF energy surfaces of  $T=0$  nuclei with SIII interaction are shown for nuclei with the mass  $A=16\sim 56$ . The proton, neutron and mass deformation parameters  $\beta_{2p}$ ,  $\beta_{2n}$  and  $\beta_2$  at the minimum of the energy surface are defined by

$$\beta_{2p} = \sqrt{\frac{\pi}{5}} \frac{Q_{2p}}{Z \langle r^2 \rangle_p} \quad (10)$$

$$\beta_{2n} = \sqrt{\frac{\pi}{5}} \frac{Q_{2n}}{N \langle r^2 \rangle_n} \quad (11)$$

$$\beta_2 = \sqrt{\frac{\pi}{5}} \frac{Q_2}{A \langle r^2 \rangle_m} \quad (12)$$

where  $\langle r^2 \rangle_p$ ,  $\langle r^2 \rangle_n$  and  $\langle r^2 \rangle_m$  are the proton, neutron and mass mean square radius, respectively. The calculated deformation parameters are tabulated in Table I for SIII and SGII interactions together with the intrinsic proton and neutron quadrupole moments  $Q_{2p}$  and  $Q_{2n}$ . The shape isomers are also found in several nuclei at low energies, which are also tabulated in Table I. The sign of deformation is always the same for protons and neutrons in a given configuration of each nucleus, while the magnitude is largely different in several configurations.

An interplay between the single particle energy gap around the Fermi surface and the quadrupole vibration energy plays an essential role to drive the deformation. As is expected from the large energy gaps at the closed shells with  $N=Z=8$  and  $N=Z=20$ , the doubly closed shell nuclei  $^{16}\text{O}$  and  $^{40}\text{Ca}$  show spherical shapes. The prolate deformations grow in  $^{20}\text{Ne}$  and  $^{24}\text{Mg}$ . In the middle of the two closed shells, the prolate and the oblate shapes are competing in  $^{28}\text{Si}$  and  $^{32}\text{S}$  so that the energy surfaces become rather flat. Just before the end of the closed shell  $N=Z=20$ , the oblate shape appears as the ground state configuration of  $^{36}\text{Ar}$ . Above the mass  $A=40$ , the prolate deformations are dominant in  $^{44}\text{Ti}$ ,  $^{48}\text{Cr}$  and  $^{52}\text{Fe}$ . Then the shape becomes again spherical in a closed shell nucleus  $^{56}\text{Ni}$ . The local oblate minima are found at low excited energies in the three nuclei  $A=44, 48$  and  $52$ . Since

the slopes of  $K=1/2^-$  and  $K=3/2^-$  states from  $f_{7/2}$  orbit go downward steeper in the the prolate side, as can be seen in Fig. 1, the prolate deformations are favored in the ground states of these nuclei. On the other hand, in the nuclei  $A=28, 32$  and  $38$ , the whole  $sd$  shell orbits are involved and give the competition between oblate and prolate deformations. In  $^{44}\text{Ti}$ , it is found that the prolate and the oblate minima are almost degenerate in energy. However the two energy minima are very shallow and have small deformations so that the dynamical fluctuations will dominate low excitation energy spectra and it is unlikely to have any rotational bands.

The calculated  $Q_{2p}$  moments are compared with experimental data in Fig. 3. The experimental  $Q_{2p}$  moments are extracted from the transition strength  $B(E2)$  between the ground states and the first excited  $2^+$  states by using Eq. (8). A clear manifestation of dynamical evolution of deformation can be seen in both the theoretical and experimental  $Q_{2p}$  moments. Namely, the  $Q_{2p}$  moment is very small in the closed shell nucleus with  $A=16$ . Then it increases when few particles are added to the closed core and shows a kind of plateau at the middle of the shells. A similar pattern is seen in the nuclei between  $A=40$  and  $56$ . Quantitatively, the calculated  $Q_{2p}$  moments are about 10~20% smaller than the empirical one in nuclei with  $A=20-36$ . However, the agreement is better in  $pf$  shell nuclei. Especially SGII interaction gives almost identical results to the empirical ones of nuclei with  $A=44-52$  within the statistical uncertainties.

It is shown that the calculated deformations of the ground states  $^{28}\text{Si}$  and  $^{36}\text{Ar}$  are oblate shapes. In both nuclei, the slopes of deformed HF single-particle energies in Fig. 1 favor the oblate deformations. As a result, in  $^{28}\text{Si}$ , the oblate shape is induced by the occupation of  $K^\pi=1/2^+$  state coming from  $1d_{5/2}$  state in the spherical limit, while the  $K^\pi=5/2^+$  state is going up rapidly in the prolate side. The oblate shape in  $^{36}\text{Ar}$  is traced back to the occupation of the  $K^\pi=3/2^+$  state coming from  $1d_{3/2}$  state in the spherical limit as well.

Deformed nuclei in the  $sd$  shell have studied with various theoretical models. As far as the quadrupole deformations of  $N=Z$  nuclei with  $A=(20\sim36)$  are concerned, the present results are very similar to the previous calculations by the HF models with various interactions [12, 13] and the modified Nilsson model [16]. Namely,  $^{20}\text{Ne}$ ,  $^{24}\text{Mg}$  and  $^{32}\text{Mg}$  were found to be prolate in the ground states, while  $^{28}\text{Si}$  and  $^{36}\text{Ar}$  are oblate. Thus, the evolution mechanism of the deformation mentioned here is common in the various microscopic models.

### C. Mass number dependence of deformations in $T=1$ nuclei

Fig. 4 shows the binding energy surfaces of nuclei with  $T=1$  with  $T_z = -1$ . The proton, neutron and mass deformation parameters  $\beta_{2p}$ ,  $\beta_{2n}$  and  $\beta_2$  at the minimum of the energy surface are tabulated in Table II for SIII and SGII interactions together with the proton and neutron quadrupole moments  $Q_{2p}$  and  $Q_{2n}$ . To study the mirror symmetry of deformations, the results of nuclei with  $T=1$  with  $T_z=1$  are also listed in Table III for SIII and SGII interactions. Since it is known that the correlations beyond the mean field approximations are important in nuclei near  $^{16}\text{O}$  and  $^{40}\text{Ca}$  [26, 27], the results of nuclei with  $A=18$  and  $40\pm2$  are shown to illustrate the systematic trend of the deformation from the beginning to the end of the shells as a manifestation of the nuclear Jahn-Teller effect. The large prolate deformations are found in  $A=22$  nuclei  $^{22}\text{Mg}$  and  $^{22}\text{Ne}$  with  $\beta_2 \sim 0.4$ . The calculated proton quadrupole moment  $Q_{2p} \sim 50 \text{ fm}^2$  ( $43 \text{ fm}^2$ ) for  $^{22}\text{Mg}$  ( $^{22}\text{Ne}$ ) shows good agreement with the empirical value  $Q_{2p} = 60 \pm 11 \text{ fm}^2$  ( $48.1 \pm 1.0 \text{ fm}^2$ ) [4]. The calculated shapes are prolate in nuclei with smaller mass than the middle of the two shell closures, i.e., in  $^{22}\text{Mg}$  and  $^{26}\text{Si}$ .

The prolate and oblate minima appear at almost the same energy in  $^{26}\text{Si}$  and  $^{26}\text{Mg}$ , while the energy surface is very flat in the case of  $^{30}\text{S}$  as can be seen in Fig. 4(b). In  $^{34}\text{Ar}$  and  $^{34}\text{S}$  having heavier mass than the middle of the two closed shells, the oblate minima are found slightly lower than the prolate ones in energy. In the  $pf$  shell nuclei, the prolate shapes dominate in the nuclei with  $A=46, 50$  and  $54$  as seen in Tables II, and III.

Fig. 5 shows the ratio  $Q_{2p}/Q_{2n}$  divided by the ratio of proton to neutron number  $Z/N$  in nuclei with  $T=1$  and  $T_z = -1$ . Because of strong proton–neutron interaction in the mean field, the value  $(Q_{2p}/Q_{2n})/(Z/N)$  becomes close to unity when the deformation is well developed. The empirical neutron deformations in the nuclei with  $T=1$   $T_z = -1$  are extracted from the proton deformations in the corresponding  $T=1$   $T_z=1$  nuclei with the same mass assuming a mirror symmetry of the deformations between the two nuclei. As far as the deformed HF calculations are concerned, the mirror symmetry of deformation is well conserved in the nuclei of  $A=(18-54)$  as seen in comparisons with Tables II and III. The ratio  $(Q_{2p}/Q_{2n})/(Z/N)$  deviates largely from unity near the doubly closed shells  $A=16$  and  $40$ . Namely the ratio is more than 2 in  $A=18$  system both in the HF calculations and the experiments. Since the driving force of deformation is only two protons in  $^{18}\text{Ne}$ , a small proton deformation is induced. While there is no neutron particles which derive the neutron deformation in  $^{18}\text{Ne}$ , the strong proton-neutron interaction raises smaller amount of deformation also for neutrons. The same trend can be seen in the nucleus with  $^{42}\text{Ti}$  having two protons top of the doubly closed shell nucleus  $^{40}\text{Ca}$ . The ratio  $(Q_{2p}/Q_{2n})/(Z/N)$  becomes opposite in the case of  $A=38$  where two neutron holes create a driving force for the deformation so that the neutron deformation is larger than the proton one although the absolute magnitude is small.

To confirm theoretical conjectures of the oblate deformations, it is necessary to obtain empirical information of the sign of the quadrupole deformation. To this end, experimental data of the quadrupole moment of excited  $2^+$  state  $Q_2(2^+)$  will be useful to determine not only the magnitude but also the sign of the intrinsic quadrupole deformation with Eq. (9). The present HF results of  $Q_2(2^+)$  are compared with experimental data and shell model calculations in Table IV. In general, the HF results show good agreement with the observed data in both the magnitude and the sign except the two nuclei  $^{18}\text{O}$  and  $^{42}\text{Ca}$  in which the correlations beyond the mean field approximation are important [26]. It is seen that the observed data show clear evidence of the oblate deformations in  $^{28}\text{Si}$  and  $^{36}\text{Ar}$ . The shell model calculations are also given in Table IV. In  $sd$  shell nuclei, the shell model results are very close to the HF ones, while we notice some differences between the two models in the  $pf$  shell nuclei. It is remarkable that our HF results give equally good or slightly better results in the  $pf$  shell nuclei compared with modern version of shell model calculations.

The two interactions give almost equivalent results in Table IV except  $^{30}\text{Si}$  in which even the sign is different. The  $Q_2(2^+)$  moments in  $^{30}\text{Si}$  and  $^{32}\text{S}$  were discussed in many mean field models [13, 18, 22] and a triaxial rotor model [23]. The HF and HF+Bogoliubov calculations with different interactions gave large positive (oblate)  $Q_2(2^+)$  in  $^{30}\text{Si}$  as was the same in the triaxial rotor model. One exception was the SII interaction which gave negative (prolate) value [12]. In Table IV, the SIII gives a negative  $Q_2(2^+)$  which is close to the shell model value, while the SGII shows a small positive value. At the moment, the accuracy of the experimental data is not good enough to distinguish which interaction or which model is better or not to predict the  $Q_2(2^+)$  moment in  $^{30}\text{Si}$ .

### III. DISCUSSIONS

#### A. Mean field models and shell models

An extensive study of deformed HF+BCS calculations was performed in ref. [32] by using SIII interaction with a seniority pairing interaction. The results in ref. [32] are quite similar to the present ones as far as the deformations of the ground states of *sd* shell nuclei  $A=16\sim 40$  are concerned. On the other hand, in  $T=0$  nuclei of *pf* shell, the results of the two calculations are different qualitatively and also quantitatively with the same Skyrme interaction SIII. In  $^{44}\text{Ti}$ , the present results with the surface  $\delta$  pairing interaction show a finite prolate deformation with  $\beta_2=0.12$  for SIII interaction and  $\beta_2=0.19$  for SGII interaction, while the result in ref. [32] shows no sign of deformation. For  $Q_{2p}$  and  $Q_{2n}$  values in  $^{48}\text{Cr}$  and  $^{52}\text{Fe}$ , the present results are (20~30)% larger than those of ref. [32] and close to the empirical values as shown in Fig. 3. For *pf* shell nuclei with  $T=1$ , the present results show finite prolate deformations  $\beta_2 \sim 0.2$  for  $^{46}\text{Cr}$  and  $\beta_2 \sim 0.12$  for  $^{54}\text{Ni}$ , while the results of ref. [32] are spherical in both cases. The  $Q_2$  moments of the present results in  $^{50}\text{Fe}$  are about 25% larger than that of ref. [32] and show better agreement with experimental data.

The magnitude of the quadrupole deformation depends on the strength of the pairing interaction. In Fig. 6, the energy surfaces of  $^{46}\text{Cr}$  are shown changing the pairing strength multiplying a factor 0.0~1.2 by the surface type pairing interaction (3). Without pairing correlation, the energy minimum appears at  $\beta_2 \sim 0.3$ . The energy minimum becomes shallower having smaller  $\beta_2$  when the pairing strength is increased. The adopted pairing strength (in the case of the factor 1.0) in this study gives the minimum at  $\beta_2=0.2$ . As is expected, the binding energy becomes larger with stronger pairing interaction. The pairing gain energy is about -16MeV in  $^{46}\text{Cr}$  and the calculated total binding energies with the adopted pairing (3) are  $E=-380\text{MeV}$  in  $^{46}\text{Cr}$  which is close to the empirical one  $E(\text{exp})=-382\text{MeV}$ . As far as the pairing gain energy is concerned, the pairing correlation is about 20% stronger in ref. [32] which gives in general smaller deformations in *pf* shell nuclei and predicts spherical shapes in some nuclei like  $^{46}\text{Cr}$  and  $^{52}\text{Fe}$ .

The Skyrme HF calculations of  $T=0$  nuclei with  $A=32\sim 48$  were performed in ref.[33] on the symmetry unrestricted basis without pairing correlations. They found a similar isotope dependence of the quadrupole deformations to that of the present calculations with the pairing correlations. They pointed out also that the octupole deformation is very small in the ground state configurations of the  $T=0$  nuclei.

The proton and neutron transition matrix elements  $M_p$ ,  $M_n$  were calculated by the shell models in *sd* shell nuclei by Brown and Wildenthal [28] and in *pf* shell nuclei by Honma et al.,[29]. The ratio of the Q moments ( $Q_{2p}/Q_{2n}$ ) of the shell models is obtained by using an equation with the values  $M_p$ ,  $M_n$  of  $T=1$ ,  $T_z = -1$  nuclei,

$$(Q_p/Q_n) = (e_p^{eff}M_p + e_n^{eff}M_n)/(e_p^{eff}M_n + e_n^{eff}M_p), \quad (13)$$

which corresponds to the ratio of transition matrices between the mirror nuclei with  $T=1$ ,  $T_z = -1$  and  $T=1$ ,  $T_z = 1$ . The effective charges are taken to be  $e_p^{eff}=1.35$  and  $e_n^{eff}=0.35$  for *sd* shell nuclei, and  $e_p^{eff}=1.5$  and  $e_n^{eff}=0.5$  for *pf* shell nuclei. In general, the mass number dependence of the shell model values  $(Q_{2p}/Q_{2n})/(Z/N)$  in Fig. 5 is similar to that of the HF results. Namely, in *sd* shell, the absolute values  $(Q_{2p}/Q_{2n})/(Z/N)$  of the shell model calculations are close to those of HF calculations and show good agreement with empirical data except the nuclei with  $A=18$  and 38. The shell model results deviate from



unity much larger than those of HF and also empirical ones in the nuclei near the closed shells  $N=Z=8$ ,  $N=Z=20$  and  $N=Z=28$  as seen in Fig. 5. The shell model transition matrix elements depend largely on the adopted model space for nuclei near the closed shell. In the case of  $A=18$ , a complete basis of  $(1p_{1/2}, 1d_{1/2}, 2s_{1/2})$  model space (so called ZBM basis) [34] gives a better result for the value  $(Q_{2p}/Q_{2n})/(Z/N)$  to be 1.67, instead of more than 3 in ref. [28], in comparison with the empirical data.

In  $pf$  shell nuclei, the shell model results are close to those of HF calculations and consistent with the empirical values in the nuclei with  $A=46$  and 50. On the other hand, the shell model values are much larger in  $A=42$  and smaller in  $A=54$  in comparison with the HF results. These results suggest that a strong proton–neutron interaction in the HF calculations induces smaller asymmetries in the deformations between  $T=1$ ,  $T_z = \pm 1$  nuclei near the closed shells than expected from the shell model results. In the middle of the closed shells, both the HF and shell model calculations give reasonable collective transition strength compared with the experimental values.

Finite-range droplet model (FRDM) has been known to provide useful information on the masses and the deformations of nuclei in a very wide region of the mass table [17]. Compared with the HF model, the FRDM gives quite different results for the quadrupole deformations in many  $sd$  and  $pf$  shell nuclei. For examples, the FRDM gives large deformations  $\beta_2=(0.32\sim 0.37)$  for  $^{20,22}\text{Ne}$  and  $^{22,24}\text{Mg}$  which are consistent with the HF results in Tables I,II,III. A nucleus  $^{26}\text{Mg}$  is predicted as an oblate shape in FRDM, while the oblate and the prolate minima are almost degenerate in the HF results in Table III. The S, Ar, Cr and Fe isotopes show substantial deformations in the HF calculations, while these isotopes are predicted to be spherical in the FRDM. It seems that the FRDM might not give proper deformations in these medium mass nuclei in comparison with empirical information discussed in this paper.

## B. New Experimental Data and Comparisons with Theories

Recently, the  $B(E2)$  values of several proton-rich unstable  $pf$  shell nuclei with  $T=1$  and  $T_z=-1$  are observed by Coulomb excitations [5–7]. The mirror symmetry in  $T=1$  nuclei with  $A=46, 50$  and 54 is experimentally confirmed by these new data. Namely, in  $A=46$ , the experimental values are  $B(E2)=(950\pm 50) e^2 fm^4$  in  $^{46}\text{Ti}$  and  $(929\pm 199) e^2 fm^4$  in  $^{46}\text{Cr}$ , while the calculated values are  $B(E2)=582.1 e^2 fm^4$  and  $913.7 e^2 fm^4$  for  $^{46}\text{Ti}$  and  $^{46}\text{Cr}$ , respectively, with SGII interaction. The different calculated  $Q$  moments of the two nuclei are due to the proton skin effect in  $^{46}\text{Cr}$  which enhances the value as is expected from Eq. 10. Experimental data of  $T=1$  and  $T_z=-1$  nuclei with  $A=50$  and 54 were reported to be  $B(E2)=(1359\pm 261) e^2 fm^4$  for  $^{50}\text{Fe}$  and  $B(E2)=(590\pm 168) e^2 fm^4$  for  $^{54}\text{Ni}$  in ref. [7]. Corresponding experimental values for  $T=1$  and  $T_z=1$  nuclei are  $B(E2)=(1080\pm 60) e^2 fm^4$  for  $^{50}\text{Cr}$  and  $B(E2)=(620\pm 50) e^2 fm^4$  for  $^{54}\text{Fe}$  [4], respectively. Calculated HF values of  $A=50$  nuclei with SGII interaction,  $B(E2)=1160 e^2 fm^4$  for  $^{50}\text{Fe}$  and  $1097 e^2 fm^4$  for  $^{50}\text{Cr}$ , show a clear mirror symmetry and give good accounts of the experimental data. The mirror symmetry is also seen in the HF calculations of  $A=54$  nuclei with  $B(E2)=373 e^2 fm^4$  for  $^{54}\text{Ni}$  and  $390 e^2 fm^4$  for  $^{54}\text{Fe}$ , although the absolute values are smaller than the observed ones. In refs. [5, 6], the  $B(E2)$  values for the ground states to the first  $2^+$  states were observed by the intermediate Coulomb excitations which give almost identical results given in refs. [4] and [7];  $B(E2)=(626\pm 169) e^2 fm^4$  for  $^{54}\text{Ni}$  and  $(640\pm 13) e^2 fm^4$  for  $^{54}\text{Fe}$ .

Shell model calculations of  $B(E2)$  strength from the ground states to the first excited

states of  $A=50$  and  $54$  nuclei were performed in a restricted  $pf$  shell model space with GXPF1 effective interaction [29]. Taking the effective charges  $e_p=1.5$  and  $e_n=0.5$ , the shell model calculations give a good mirror symmetry in the case of  $A=50$  nuclei with  $B(E2)=910 e^2 fm^4$  for  $^{50}Cr$  and  $B(E2)=954 e^2 fm^4$  for  $^{50}Fe$  although the absolute values are somewhat smaller than the experimental values and those of deformed HF calculations with SGII interaction. The shell model gives a reasonable  $B(E2)$  value for  $^{54}Fe$  to be  $B(E2)=651 e^2 fm^4$ , while the calculated value is smaller than the experimental one in the case of  $^{54}Ni$  as  $B(E2)=324 e^2 fm^4$ .

If the mean square radii are close  $\langle r_p^2 \rangle \simeq \langle r_n^2 \rangle$  in a nucleus, the ratio  $Q_{2p}/Q_{2n}$  divided by  $Z/N$  should be the same as the ratio  $\delta_p/\delta_n$  (or equivalently  $\beta_p/\beta_n$ ). One can notice that  $T=0$  nuclei in Table I show the proportionality between  $Q$  moments and the deformation parameters  $\beta_2$  as is expected from Eqs. 10 and 11. On the other hand, in Tables II and III, the  $Q$  moments are not always proportional to the  $\beta_p$  and  $\beta_n$  values. This is due to a difference of the proton skin effect in the  $T_z = -1$  nuclei to the neutron skin effect in the  $T_z = 1$  nuclei. In Fig. 8, the calculated proton skin thickness of the ground state,

$$\delta r_{pn} = \langle r_p \rangle - \langle r_n \rangle, \quad (14)$$

is shown for the nuclei in  $sd$  and  $pf$  shell with  $T=1$  and  $T_z = \pm 1$ . The results of SGII are shown in Fig. 8. We calculated also the skin thickness by using the SIII interaction and found almost identical results to those shown in Fig. 8. In  $A=18$ , the proton-rich nucleus  $^{18}Ne$  has a large proton skin and the neutron-rich nucleus  $^{18}O$  has an equally large neutron skin. The large skin thickness is created by two particle occupation of the  $1d_{5/2}$  orbit which has much larger radius than  $1p$  orbits. The proton skin thickness of nuclei with  $T_z = -1$  decreases gradually for heavier  $pf$  shell nuclei, but still finite to be  $\delta r_{pn} \simeq 0.1$  even in  $^{54}Ni$ . The irregularity at  $A=30$  is due to the occupation of  $2s_{1/2}$  orbit. The neutron skin thickness of nuclei with  $T_z = 1$  decreases more rapidly for heavier  $sd$  shell nuclei and almost disappears in the  $pf$  shell nuclei. This difference between the nuclei with  $T_z = \pm 1$  is due to the effect of the Coulomb interaction on the mean field proton potential. Since the Coulomb potential makes shallower proton HF potential in  $pf$  shell nuclei, the extra two protons give always the enhancement of the proton rms radii in  $T_z = -1$  nuclei. On the other hand, the neutron potential is deeper than the proton one in  $T_z = 1$  nuclei so that the extra two neutrons do not create appreciable neutron skin in  $pf$  shell nuclei. This difference of the skin thickness gives rise to a substantial effect on the  $Q$  moment. One of the clear examples of the skin effect is seen in  $^{50}Fe$  where the proton deformation is smaller than the neutron one, but the  $Q_{2p}$  moment is larger than  $Q_{2n}$  moment.

### C. Hexadecapole deformation in $sd$ and $pf$ shell nuclei

Higher multipole deformations such as the hexadecapole deformation were discussed in ref. [12] by the Skyrme HF calculations without pairing correlations. It is an interesting subject whether the pairing correlations are important or not for the evolution of higher multipole deformations than the quadrupole. The proton and neutron hexadecapole deformations of  $T=0$  and  $T=1$  nuclei are listed in Tables I, II and III. In  $sd$  shell nuclei, a large  $Q_4$  in  $^{20}Ne$  and a small  $Q_4$  in  $^{24}Mg$  are expected as the shell filling effect in prolate deformed potential [9, 12]. The present HF results are consistent with the shell filling effect. The two interactions SIII and SGII give a large difference in the  $Q_4$  moment of  $^{28}Si$ . In comparison

with experimental data in Fig. 7, SGII gives a better prediction in  $^{28}\text{Si}$ . In  $^{32}\text{S}$  and  $^{36}\text{Ar}$ , the calculated  $Q_4$  moments are relatively small compared with other  $sd$  shell nuclei, while the shell model gives several times larger  $Q_4$  moments in these two nuclei [37]. We need more data, for example, by electron scatterings, to compare with these calculated results in  $^{32}\text{S}$  and  $^{36}\text{Ar}$ , although the proton scattering data of  $^{32}\text{S}$  show an indication of large  $Q_{4p}$  value [38].

For  $pf$  shell nuclei, the  $Q_4$  moments increase drastically from  $^{44}\text{Ti}$  and peaked at  $^{48}\text{Cr}$ . In the heavier  $pf$  shell nuclei, we can see a large drop in magnitude of  $Q_4$  moment from  $^{48}\text{Cr}$  to  $^{56}\text{Ni}$ . In general, SGII gives larger  $Q_4$  moments in  $pf$  shell than SIII. In  $sd$  shell nuclei, the HF results underestimate somewhat the empirical values, while the calculations give reasonable values of  $Q_4$  moment in  $pf$  shell nuclei,  $^{46}\text{Ti}$  and  $^{50}\text{Cr}$ .

#### IV. SUMMARY

We pointed out the strong mass number dependence of quadrupole deformations in the nuclei with mass  $A=(16\sim 56)$  as a clear manifestation of the evolution of nuclear deformation in atomic nuclei by using the deformed HF+BCS calculations. The effect in the medium-heavy nuclei is unique to compare with that in rare-earth nuclei since the prolate and oblate deformations appear clearly in the ground states depending on the Fermi energy in the deformed single-particle energy levels. It is shown that the deformed HF+BCS model is successful to describe observed  $Q_2$  and  $Q_4$  moments of the nuclei with the isospin  $T=0$  and  $T=1$  in  $sd$  and  $pf$  shell in the same level as modern shell model calculations. The isospin symmetry of quadrupole deformations of mirror nuclei with  $T=1$ ,  $T_z = \pm 1$  is studied in comparison with the empirical data and the shell model calculations. It was shown that the value  $(Q_{2p}/Q_{2n})/(Z/N)$  is close to unity in the well-deformed nuclei in the middle of the shell, while the values deviate largely from the unity in nuclei near the closed shell both in the HF calculations and also in the empirical values. The HF results show oblate shapes in some  $sd$  shell nuclei and the available observed  $Q_2(2^+)$  moments of the first excited states are consistent with the theoretical predictions. The effect of the pairing interaction on the deformation is carefully examined by changing the pairing strength. We point out also the effect of large proton skin thickness on the  $Q_2$  moments in the  $N\sim Z$  nuclei.

#### Acknowledgments

We thank T. Motobayashi and K. Yamada for showing their data prior to a publication. We thank also M. Honma for providing the results of his shell model calculations. We are benefited from discussions with I. Hamamoto and K. Matsuyanagi. This work is supported in part by the Japanese Ministry of Education, Culture, Sports, Science and Technology by Grant-in-Aid for Scientific Research under the program number (C(2)) 16540259.

- 
- [1] H. A. Jahn and E. Teller, Proc. Roy. Soc. **A161**, 220 (1937).
  - [2] P. -G. Reinhard and E. W. Otten, Nucl. Phys. **A420**, 173 (1984).
  - [3] W. Nazarewicz, Int. Jour. Mod. Phys. **E2**, 51 (1993); Nucl. Phys. **A574**, 27c (1994).
  - [4] S. Raman, C. W. Nestor, Jr. and P. Tikkanen, Atomic Data Nucl. Data Tables **78**, 1 (2001).

- [5] K. L. Yurkewicz et al., Phys. Rev. **C70** 034301 (2004).
- [6] K. L. Yurkewicz et al., Phys. Rev. **C70** 054319 (2004).
- [7] K. Yamada et al., Proc. of ENAM04 (Callaway Gardens, 2004);  
K. Yamada, Ph.D. Thesis (Rikkyo University, 2004).
- [8] T. Koike, K. Starosta and I. Hamamoto, Phys. Rev. Lett. **93** 172502 (2004).
- [9] A. Bohr and B. R. Mottelson, Nuclear Structure Vol. 2 (1975, W. A. Benjamin, Inc., New York).
- [10] N. Tajima and N. Suzuki, Phys. Rev. **C64** 037301 (2001).
- [11] H. Sagawa, X. R. Zhou, X. Z. Zhang and T. Suzuki, Phys. Rev. **C70**, 054316 (2004).
- [12] H. R. Jacaman and L. Zamick, Phys. Rev. **C30**, 1719 (1984).
- [13] P. Quantin and H. Flocard, Ann. Rev. Nucl. Part. Science **28**, 523 (1978).
- [14] S. Aberg, H. Flocard and W. Nazarewicz, Ann. Rev. Nucl. Part. Science **40** 439, (1990).
- [15] I. Ragnarsson and R. K. Sheline, Phys. Scripta **29**, 385 (1984).
- [16] I. Ragnarsson, S. Aberg and R. K. Sheline, Phys. Scripta **24**, 215 (1981).
- [17] P. Möller, J. R. Nix, W. D. Myers and W. J. Swiatecki, Atomic Data and Nuclear Data Tables, **59**, 185 (1995).
- [18] B. Castel and J. C. Parikh, Phys. Lett. **29B**, 341 (1969).
- [19] H. Flocard, P. Quantin, A. K. Kerman and D. Vautherin, Nucl. Phys. **A203**, 433 (1973).
- [20] P. Bonche, H. Flocard, P. H. Heenen, S. J. Krieger and M. S. Weiss, Nucl. Phys. **A443**, 39 (1985); P. Bonche, H. Flocard and P. H. Heenen, Nucl. Phys. **AA467**, 115 (1987).
- [21] M. Girod and B. Grammaticos, Phys. Rev. **C27**, 2317 (1983).
- [22] K. Goeke, A. Faessler and H. H. Wolter, Nucl. Phys. **A183**, 352 (1972); K. Goeke, J. Garcia and A. Faessler, Nucl. Phys. **A208**, 477 (1973).
- [23] D. Kurath, Phys. Rev. **C5**, 768 (1972).
- [24] T. Suzuki, H. Sagawa, and K. Hagino, in the Proceedings of the International Symposium on “Frontiers of Collective Motions (CM2002)”, (2003, World Scientific) p. 236;  
H. Sagawa, T. Suzuki and K. Hagino, Nucl. Phys. **A722**, 183 (2003); Phys. Rev. **C68**, 014317 (2003).
- [25] M. Bender, K. Rutz, P.-G. Reinhard, and J.A. Maruhn, Eur. Phys. J. **A8**, 59 (2000).
- [26] M. Bender, H. Flocard and P.-H. Heenen, Phys. Rev. **C68**, 044321 (2003).
- [27] E. Caurier, K. Langanke, G. Martinez-Pinedo, F. Nowacki and P. Vogel, Phys. Lett. B **522**, 240 (2001).
- [28] B. A. Brown, B. H. Wildenthal, W. Chung, S. E. Masses, M. Bernas, A. M. Bernstein, R. Miskimen, V. R. Brown and V. A. Madsen, Phys. Rev. **C26**, 2247 (1982).
- [29] M. Honma, T. Otsuka, B. A. Brown and T. Mizusaki, Phys. Rev. **C69**, 034335 (2004) and private communications.
- [30] B. H. Wildenthal, J. B. McGrory and P. W. M. Glaudemans, Phys. Rev. Lett. **26**, 96 (1971).
- [31] P. Raghavan, Atomic and Nucl. Data Tables **42**, 189 (1989)
- [32] N. Tajima, S. Takahara and N. Onishi, Nucl. Phys. **A603**, 23 (1996) and private communications.
- [33] T. Inakura, S. Mizutori, M. Yamagami and K. Matsuyanagi, Nucl. Phys. **A710**, 261 (2002).
- [34] A. P. Zucker, F. A. Buck and J. B. McGrory, Phys. Rev. Lett. **21**, 39 (1968).
- [35] P. M. Endt, Atomic and Nucl. Data Tables **55**, 171 (1993); J. W. Lightbody et al., Phys. Rev. **C27**, 113 (1983).
- [36] NNDC World Wide web site from the ENSDF database.
- [37] B. A. Brown, W. Chung and B. H. Wildenthal, Phys. Rev. **C21**, 2600 (1980).

- [38] R. De Leo, G. D'Erasmus, A. Pantaleo, M. N. Harakeh, S. Micheletti and M. Pignanelli, Phys. Rev.**C23**, 1355 (1981).

## Figures

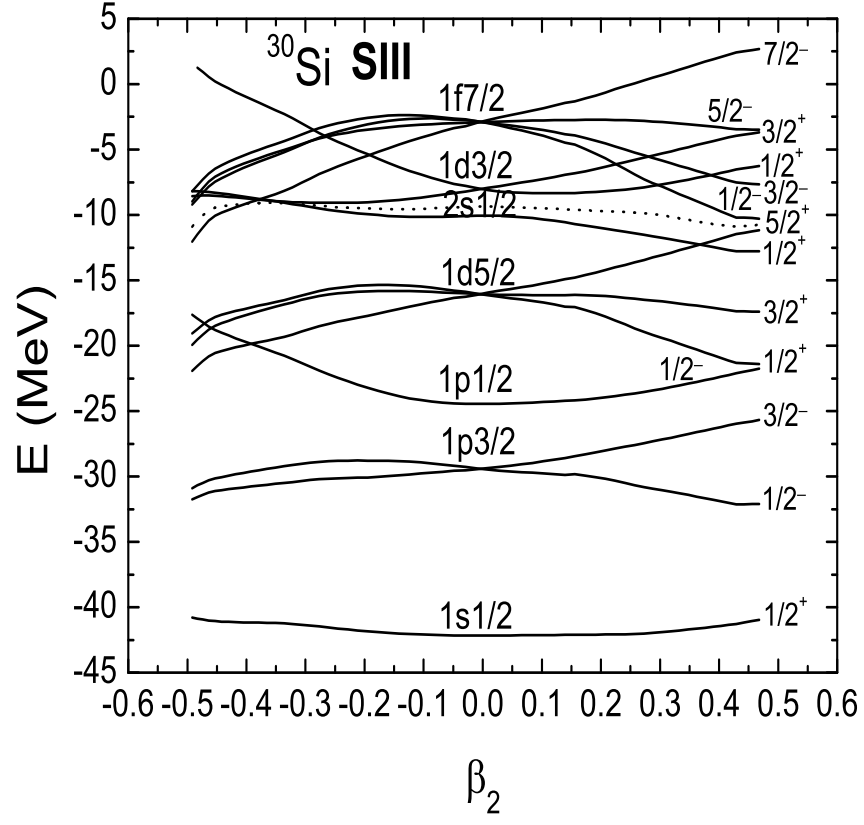


FIG. 1: Neutron HF single particle energies as a function of the deformation parameter  $\beta_2$  in  $^{30}\text{Si}$ . The deformed HF calculations are performed by using SIII interaction.

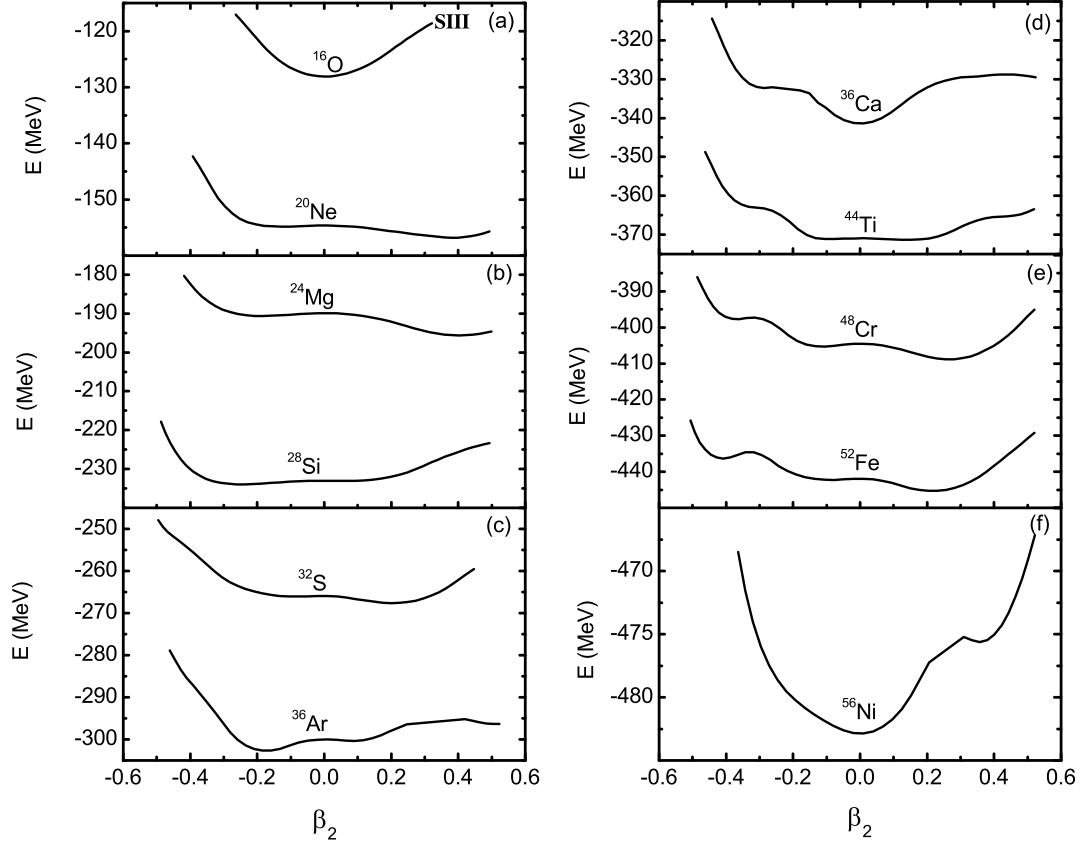


FIG. 2: Deformed HF + BCS calculations of T=0 nuclei with SIII interaction; (a) for  $^{16}\text{O}$  and  $^{20}\text{Ne}$ , (b) for  $^{24}\text{Mg}$  and  $^{28}\text{Si}$ , (c) for  $^{32}\text{S}$  and  $^{36}\text{Ar}$ , (d) for  $^{36}\text{Ca}$  and  $^{44}\text{Ti}$ , (e) for  $^{48}\text{Cr}$  and  $^{52}\text{Fe}$  and (f) for  $^{56}\text{Ni}$ . The density dependent pairing interaction (3) is adopted in the calculations.

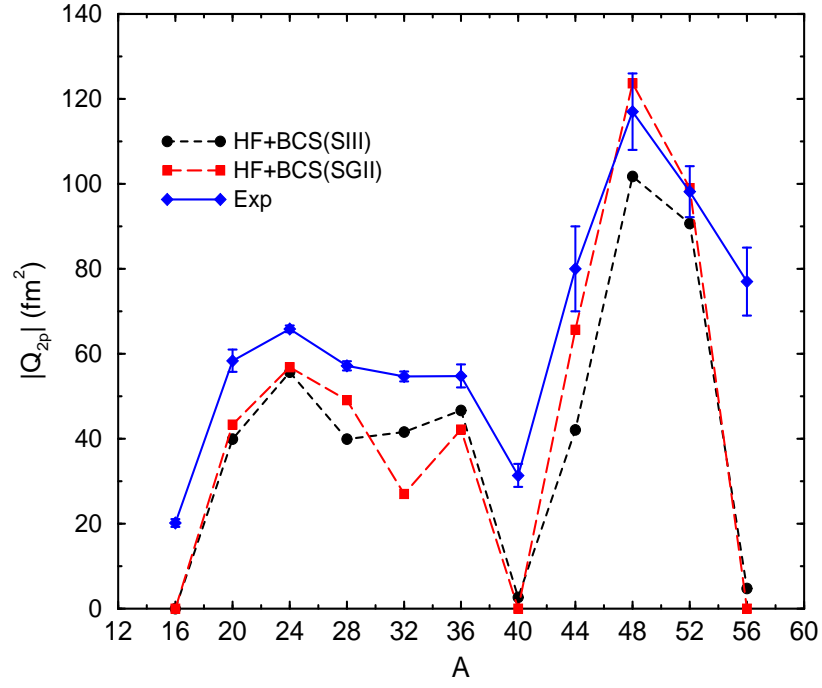


FIG. 3: Absolute values of proton quadrupole moments in *sd* and *pf* shell nuclei with  $N=Z$ . Deformed HF + BCS calculations are performed with SIII and SGII interactions. The density dependent pairing interaction (3) is adopted in the calculations. The experimental data are taken from refs. [4, 7].



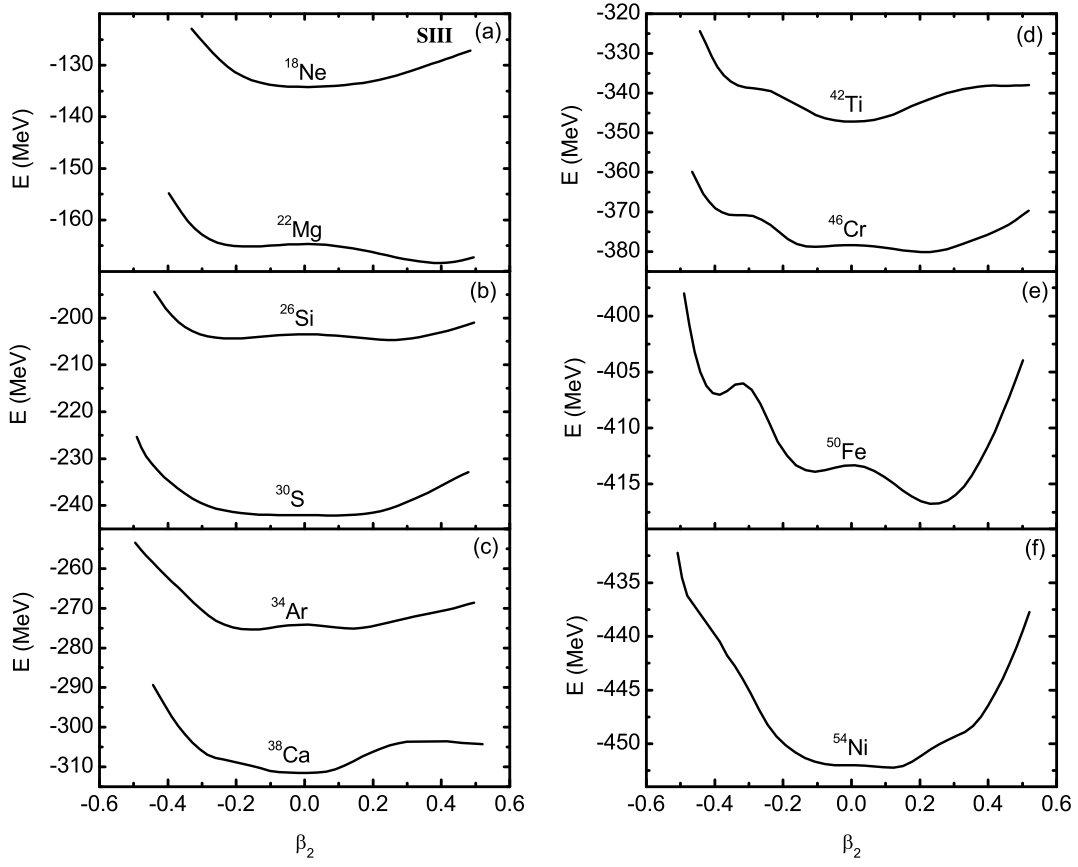


FIG. 4: Deformed HF + BCS calculations of  $T=1$  with SIII interaction; (a) for  $^{18}\text{Ne}$  and  $^{22}\text{Mg}$ , (b) for  $^{26}\text{Si}$  and  $^{30}\text{S}$ , (c) for  $^{34}\text{Ar}$  and  $^{38}\text{Ca}$ , (d) for  $^{42}\text{Ti}$  and  $^{46}\text{Cr}$ , (e) for  $^{50}\text{Fe}$  and (f) for  $^{54}\text{Ni}$ . The density dependent pairing interaction (3) is adopted in the calculations.

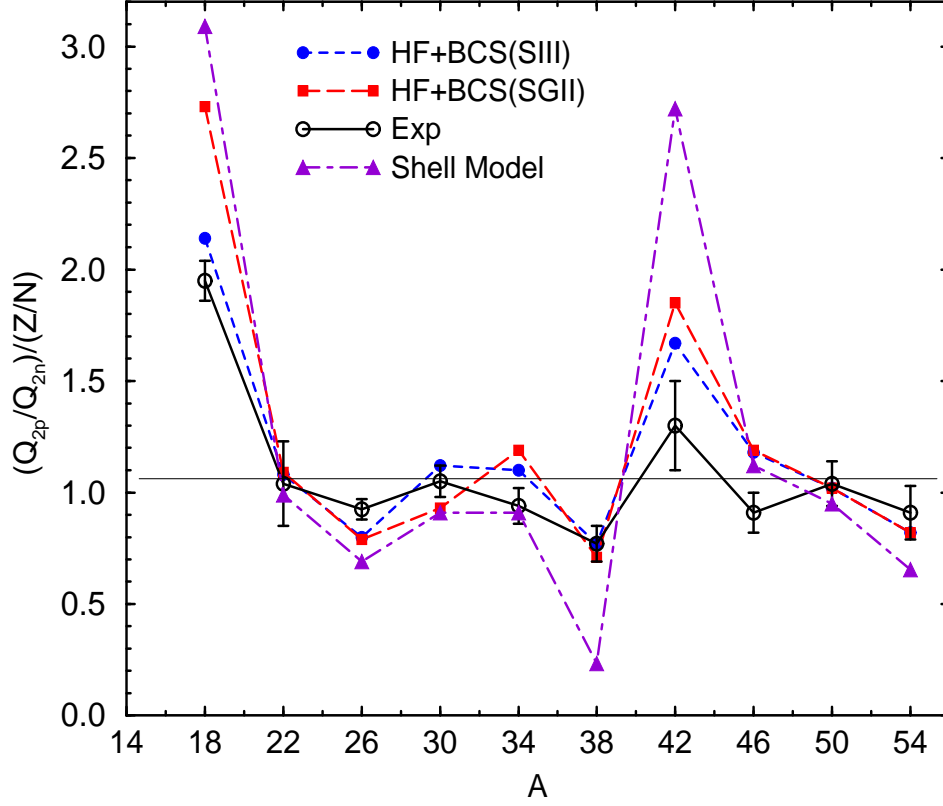


FIG. 5: Ratio of proton to neutron quadrupole moments ( $Q_{2p}/Q_{2n}$ ) divided by that of proton to neutron numbers ( $Z/N$ ) in  $sd$  and  $pf$  shell nuclei with  $T=1$  and  $T_z = -1$ . Deformed HF + BCS calculations are performed with SIII and SGII interactions. The density dependent pairing interaction (3) is adopted in the HF calculations. The shell model values are calculated by using Eq. (13). The shell model transition matrices of  $sd$  shell are taken from ref. [28], while those of  $pf$  shell are taken from ref. [29]. The empirical values are obtained by assuming a mirror symmetry between proton and neutron quadrupole moments in  $T=1$  and  $T_z = \pm 1$  nuclei with the same mass number  $A$ . Experimental data are taken from refs. [4, 7]. See the text for details.

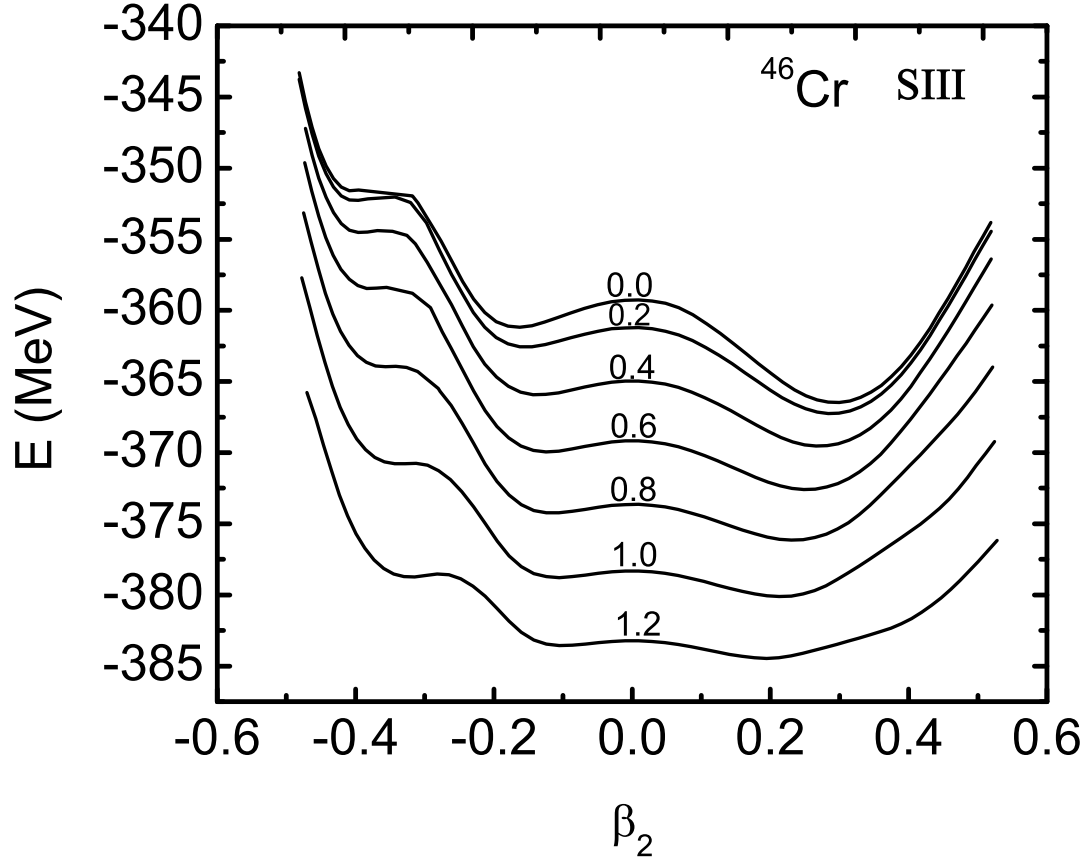


FIG. 6: Deformed HF + BCS calculations of  $^{46}\text{Cr}$  with different pairing strength multiplying a factor 0.0~1.2 to the surface type pairing interaction (3). The SIII interaction is used.

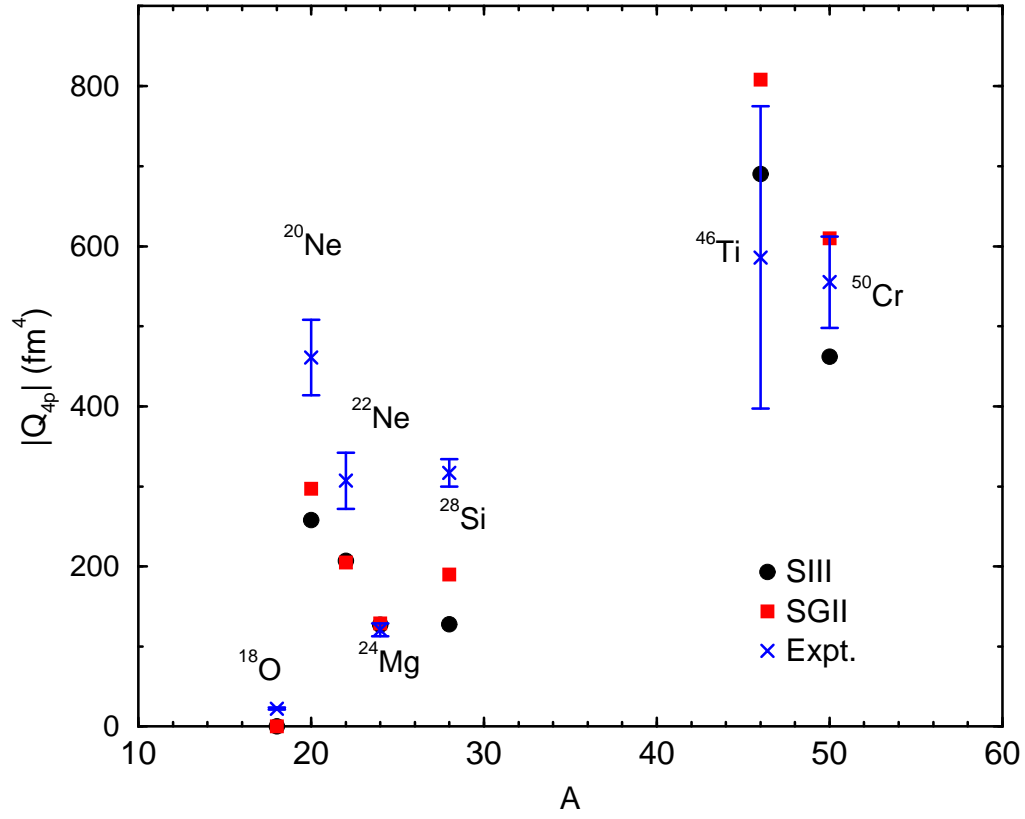


FIG. 7: Proton hexadecapole moment  $Q_{4p}$  defined by Eq. (6). The SIII and SGII interactions are used in the deformed HF calculations with a surface pairing interaction (3). Experimental data are taken from refs. [35, 36]. See the text for details.

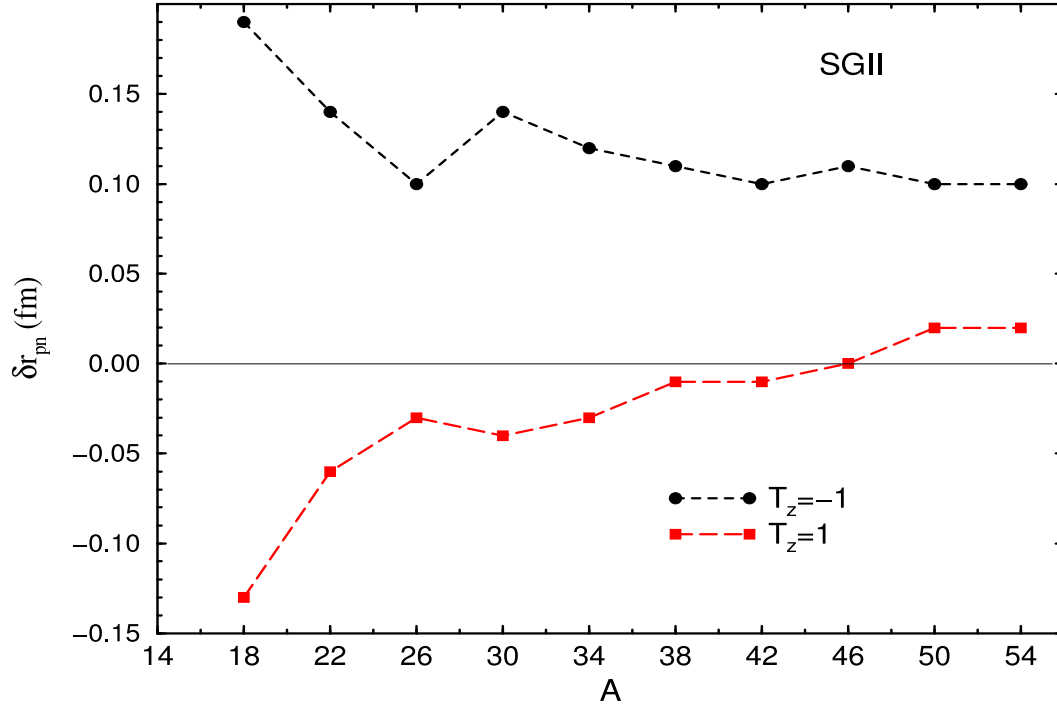


FIG. 8: The difference between proton and neutron rms radii defined by Eq. (14). The SGII interaction is used in the deformed HF calculations with a surface pairing interaction (3). See the text for details.

TABLE I: Quadrupole deformation parameters  $\beta_2$ , quadrupole moments  $Q_2$  and hexadecapole moments  $Q_4$  in  $sd$  and  $pf$  shell nuclei with the isospin  $T=0$ . The deformed HF+BCS calculations are performed with SIII and SGII interactions together with the density dependent pairing interaction (3). The axial symmetry is assumed in the HF calculations. The proton, neutron and mass deformation parameters ( $\beta_{2p}$ ,  $\beta_{2n}$  and  $\beta_2$ ) are obtained at the energy minima of protons, neutron and mass potentials, respectively. The proton and neutron quadrupole and hexadecapole moments are calculated by using deformed HF wave functions at each energy minima. The local minima of the energy surfaces at low excitation energies are also listed.

SIII	$K^\pi$	Energy (MeV)	$\beta_{2p}$	$\beta_{2n}$	$\beta_2$	$Q_{2p}$ ( $fm^2$ )	$Q_{2n}$ ( $fm^2$ )	$Q_{4p}$ ( $fm^4$ )	$Q_{4n}$ ( $fm^4$ )
$^{16}O$	$0^+$	0.0	0.0	0.0	0.0	-0.01	-0.01	-0.15	-0.15
$^{20}Ne$	$0^+$	0.0	0.38	0.34	0.38	39.93	38.87	257.58	243.63
	$0^+$	1.98	-0.13	-0.13	-0.13	-12.94	-12.55	21.32	20.03
$^{24}Mg$	$0^+$	0.0	0.40	0.40	0.40	55.71	54.43	126.63	123.57
$^{28}Si$	$0^+$	0.0	-0.24	-0.24	-0.24	-39.97	-38.88	127.61	120.73
	$0^+$	0.86	0.04	0.04	0.04	6.10	5.92	7.28	6.74
$^{32}S$	$0^+$	0.0	0.20	0.20	0.20	41.62	40.10	-49.84	-44.64
	$0^+$	1.54	-0.08	-0.08	-0.08	-16.40	-15.59	-8.82	-7.84
$^{36}Ar$	$0^+$	0.0	-0.18	-0.18	-0.18	-44.46	-43.01	-47.34	-41.74
	$0^+$	2.30	0.09	0.09	0.09	22.59	22.01	-15.62	-13.92
$^{40}Ca$	$0^+$	0.0	0.01	0.01	0.01	2.72	2.64	1.17	0.97
$^{44}Ti$	$0^+$	0.0	0.15	0.15	0.15	51.73	49.96	508.84	467.90
	$0^+$	0.20	-0.11	-0.11	-0.11	-35.78	-34.80	155.90	144.70
$^{48}Cr$	$0^+$	0.0	0.26	0.26	0.26	101.80	98.72	785.70	737.63
	$0^+$	3.55	-0.11	-0.11	-0.11	-41.17	-39.86	40.45	35.71
$^{52}Fe$	$0^+$	0.0	0.20	0.20	0.20	90.72	88.19	-27.00	-16.71
	$0^+$	3.04	-0.08	-0.08	-0.08	-34.16	-33.22	-32.77	-29.07
$^{56}Ni$	$0^+$	0.0	0.01	0.01	0.01	4.78	4.63	-12.13	-11.04

SGII	$K^\pi$	Energy (MeV)	$\beta_{2p}$	$\beta_{2n}$	$\beta_2$	$Q_{2p}$ ( $fm^2$ )	$Q_{2n}$ ( $fm^2$ )	$Q_{4p}$ ( $fm^4$ )	$Q_{4n}$ ( $fm^4$ )
$^{16}O$	$0^+$	0.0	0.0	0.0	0.0	-0.01	-0.01	-0.17	-0.17
$^{20}Ne$	$0^+$	0.0	0.41	0.41	0.41	43.38	42.12	297.09	279.87
	$0^+$	2.69	-0.15	-0.15	-0.15	-14.81	-14.33	29.61	27.60
$^{24}Mg$	$0^+$	0.0	0.42	0.42	0.42	56.88	55.42	129.01	125.44
$^{28}Si$	$0^+$	0.0	-0.29	-0.29	-0.29	-49.12	-47.58	190.08	178.53
	$0^+$	1.97	0.10	0.10	0.10	15.11	14.67	21.40	20.01
$^{32}S$	$0^+$	0.0	0.14	0.13	0.13	27.04	25.83	-27.16	-24.14
$^{36}Ar$	$0^+$	0.0	-0.17	-0.17	-0.17	-42.21	-40.66	-64.86	-57.59
	$0^+$	1.63	0.09	0.09	0.09	22.45	21.85	-15.14	-13.26
$^{40}Ca$	$0^+$	0.0	0.0	0.0	0.0	0.03	0.04	0.05	0.03
$^{44}Ti$	$0^+$	0.0	0.19	0.19	0.19	65.48	62.80	823.01	750.34
	$0^+$	0.68	-0.10	-0.10	-0.10	-32.54	-31.59	140.74	130.16
$^{48}Cr$	$0^+$	0.0	0.31	0.31	0.31	123.69	119.18	1057.68	985.81
	$0^+$	4.46	-0.12	-0.12	-0.12	-44.72	-43.38	52.80	50.20
$^{52}Fe$	$0^+$	0.0	0.23	0.23	0.23	99.0	95.85	49.32	55.63
	$0^+$	3.72	-0.12	-0.12	-0.12	-51.23	-49.57	106.35	98.11
$^{56}Ni$	$0^+$	0.0	0.0	0.0	0.0	-0.01	-0.0	-60.41	-54.23

TABLE II: Quadrupole deformation parameters  $\beta_2$ , quadrupole moments  $Q_2$  and hexadecapole moments  $Q_4$  in  $sd$  and  $pf$  shell nuclei with the isospin  $T=1$  and  $T_z = -1$ . The deformed HF+BCS calculations are performed with SIII and SGII interactions together with the density-dependent pairing interaction. See the caption to Table I for details.

SIII	$K^\pi$	Energy (MeV)	$\beta_{2p}$	$\beta_{2n}$	$\beta_2$	$Q_{2p}$ ( $fm^2$ )	$Q_{2n}$ ( $fm^2$ )	$Q_{4p}$ ( $fm^4$ )	$Q_{4n}$ ( $fm^4$ )
$^{18}Ne$	$0^+$	0.0	0.01	0.01	0.01	1.16	0.43	-2.87	-0.49
$^{22}Mg$	$0^+$	0.0	0.40	0.401	0.40	54.65	42.00	175.85	207.73
	$0^+$	3.16	-0.15	-0.16	-0.16	-20.26	-15.58	31.97	29.20
$^{26}Si$	$0^+$	0.0	0.21	0.28	0.24	34.88	37.53	59.15	49.84
	$0^+$	0.33	-0.21	-0.21	-0.21	-34.86	-27.63	90.01	64.14
$^{30}S$	$0^+$	0.0	0.10	0.09	0.09	19.17	15.01	1.98	10.49
$^{34}Ar$	$0^+$	0.0	-0.16	-0.16	-0.16	-39.94	-32.24	-36.68	-12.87
	$0^+$	0.21	0.13	0.16	0.14	31.38	33.45	-28.93	-26.07
$^{38}Ca$	$0^+$	0.0	0.01	0.01	0.01	2.20	2.58	0.81	1.35
$^{42}Ti$	$0^+$	0.0	0.01	0.01	0.01	3.83	2.08	-10.42	-3.26
$^{46}Cr$	$0^+$	0.0	0.21	0.19	0.20	83.97	65.13	744.56	639.78
	$0^+$	1.33	-0.11	-0.11	-0.11	-40.82	-35.16	90.35	112.74
$^{50}Fe$	$0^+$	0.0	0.23	0.24	0.23	100.19	91.12	390.70	499.18
	$0^+$	2.87	-0.10	-0.11	-0.11	-45.39	-41.56	50.28	42.44
$^{54}Ni$	$0^+$	0.0	0.11	0.14	0.12	52.96	60.37	86.04	30.38
SGII	$K^\pi$	Energy (MeV)	$\beta_{2p}$	$\beta_{2n}$	$\beta_2$	$Q_{2p}$ ( $fm^2$ )	$Q_{2n}$ ( $fm^2$ )	$Q_{4p}$ ( $fm^4$ )	$Q_{4n}$ ( $fm^4$ )
$^{18}Ne$	$0^+$	0.0	0.01	0.06	0.01	1.40	0.35	-0.42	-0.20
$^{22}Mg$	$0^+$	0.0	0.41	0.41	0.40	54.74	42.01	176.14	213.04
	$0^+$	3.63	-0.20	-0.19	-0.19	-25.62	-18.73	57.89	45.24
$^{26}Si$	$0^+$	0.0	0.24	0.318	0.27	38.47	41.49	73.97	66.93
	$0^+$	0.18	-0.24	-0.24	-0.24	-39.77	-30.80	118.14	85.27
$^{30}S$	$0^+$	0.0	-0.09	-0.11	-0.10	-17.90	-16.85	-3.26	9.88
	$0^+$	0.0	0.03	0.04	0.04	6.73	6.76	4.93	5.33
$^{34}Ar$	$0^+$	0.0	-0.13	-0.12	-0.13	-31.81	-23.86	-42.35	-26.89
	$0^+$	0.26	0.11	0.13	0.12	23.73	21.36	-16.79	-18.03
$^{38}Ca$	$0^+$	0.0	0.01	0.01	0.01	2.10	2.68	0.81	1.30
$^{42}Ti$	$0^+$	0.0	0.0	-0.00	-0.00	0.01	0.0	-4.22	-1.32
$^{46}Cr$	$0^+$	0.0	0.248	0.221	0.235	96.03	73.77	914.29	787.16
	$0^+$	2.13	-0.13	-0.13	-0.13	-48.46	-41.11	149.33	171.21
$^{50}Fe$	$0^+$	0.0	0.25	0.26	0.25	108.03	98.0	394.96	523.95
	$0^+$	3.70	-0.13	-0.13	-0.13	-54.28	-48.21	106.15	74.09
$^{54}Ni$	$0^+$	0.0	0.13	0.16	0.15	61.17	69.13	60.88	8.37
	$0^+$	0.53	-0.07	-0.08	-0.07	-31.51	-31.40	4.79	-9.09



TABLE III: Quadrupole deformation parameters  $\beta_2$ , quadrupole moments  $Q_2$  and hexadecapole moments  $Q_4$  in  $sd$  and  $pf$  shell nuclei with the isospin  $T=1$  and  $T_z = 1$ . The deformed HF+BCS calculations are performed with SIII and SGII interactions together with the density-dependent pairing interaction. See the caption to Table I for details.

SIII	$K^\pi$	Energy (MeV)	$\beta_{2p}$	$\beta_{2n}$	$\beta_2$	$Q_{2p}$ ( $fm^2$ )	$Q_{2n}$ ( $fm^2$ )	$Q_{4p}$ ( $fm^4$ )	$Q_{4n}$ ( $fm^4$ )
$^{18}O$	$0^+$	0.0	-0.01	-0.01	-0.01	-0.51	-1.00	-0.13	-0.10
$^{22}Ne$	$0^+$	0.0	0.39	0.38	0.39	41.38	51.15	206.75	159.93
	$0^+$	3.08	-0.16	-0.15	-0.16	-15.99	-19.55	30.64	30.17
$^{26}Mg$	$0^+$	0.0	0.29	0.22	0.25	39.64	35.41	59.63	64.73
	$0^+$	0.31	-0.21	-0.21	-0.21	-28.33	-33.78	66.75	84.20
$^{30}Si$	$0^+$	0.0	0.08	0.09	0.08	13.99	16.55	9.92	3.22
$^{34}S$	$0^+$	0.0	-0.16	-0.16	-0.16	-33.34	-38.41	-13.58	-29.72
	$0^+$	0.29	0.16	0.12	0.14	32.59	28.67	-27.90	-24.61
$^{38}Ar$	$0^+$	0.0	-0.01	-0.01	-0.01	-3.49	-1.78	-0.39	-0.44
$^{42}Ca$	$0^+$	0.0	-0.01	-0.01	-0.01	-2.19	-3.85	-0.88	-2.47
$^{46}Ti$	$0^+$	0.0	0.20	0.22	0.21	70.40	84.65	689.82	688.03
	$0^+$	1.29	-0.11	-0.11	-0.11	-36.09	-39.59	121.36	86.17
$^{50}Cr$	$0^+$	0.0	0.24	0.23	0.23	93.70	97.15	461.74	302.57
	$0^+$	2.81	-0.10	-0.10	-0.11	-42.66	-43.97	43.84	46.20
$^{54}Fe$	$0^+$	0.0	0.12	0.09	0.11	52.72	43.51	17.18	59.43
$^{58}Ni$	$0^+$	0.0	0.11	0.14	0.13	56.09	74.64	238.35	343.72
	$0^+$	0.17	-0.09	-0.10	-0.09	-42.38	-50.42	115.25	94.07
SGII	$K^\pi$	Energy (MeV)	$\beta_{2p}$	$\beta_{2n}$	$\beta_2$	$Q_{2p}$ ( $fm^2$ )	$Q_{2n}$ ( $fm^2$ )	$Q_{4p}$ ( $fm^4$ )	$Q_{4n}$ ( $fm^4$ )
$^{18}O$	$0^+$	0.0	0.01	0.01	0.01	0.37	1.27	-0.19	-0.27
$^{22}Ne$	$0^+$	0.0	0.41	0.40	0.41	43.19	53.21	225.14	171.92
	$0^+$	3.61	-0.18	-0.19	-0.18	-18.39	-23.47	43.48	47.64
$^{26}Mg$	$0^+$	0.0	0.32	0.24	0.28	42.59	37.48	71.51	73.05
	$0^+$	0.16	-0.24	-0.24	-0.24	-31.71	-38.40	89.68	109.92
$^{30}Si$	$0^+$	0.0	-0.02	-0.02	-0.02	-3.44	-3.57	-5.25	-6.15
$^{34}S$	$0^+$	0.0	-0.13	-0.14	-0.14	-26.93	-32.46	-27.97	-36.41
	$0^+$	0.25	0.14	0.11	0.12	27.51	25.70	-26.42	-19.14
$^{38}Ar$	$0^+$	0.0	0.01	0.01	0.01	2.69	2.11	0.38	0.15
$^{42}Ca$	$0^+$	0.0	0.01	0.01	0.01	2.0	3.83	0.64	1.78
$^{46}Ti$	$0^+$	0.0	0.22	0.25	0.24	76.50	92.14	807.53	796.05
	$0^+$	2.07	-0.11	-0.11	-0.11	-35.86	-39.73	139.57	105.34
$^{50}Cr$	$0^+$	0.0	0.27	0.26	0.26	105.20	108.17	609.74	419.16
	$0^+$	3.65	-0.14	-0.14	-0.14	-53.17	-56.62	94.77	123.07
$^{54}Fe$	$0^+$	0.0	0.15	0.11	0.13	62.84	50.50	23.90	82.27
$^{58}Ni$	$0^+$	0.0	-0.11	-0.12	-0.11	-53.14	-59.25	173.44	118.77
	$0^+$	0.02	0.12	0.14	0.13	56.64	73.71	195.14	238.98

TABLE IV: Quadrupole moments  $Q_2(2^+)$  of the first excited  $2^+$  states in  $sd$  and  $pf$  shell nuclei. The unit is  $e \cdot fm^2$ . Shell model values of  $sd$  shell nuclei are taken from ref. [30], while those of  $pf$  shell nuclei are taken from ref. [29]. Experimental data are taken from the compilation of ref. [31].

nucleus	SIII	SGII	shell model	Expt.
$^{18}\text{O}$	0.15	-0.10	-2.0	$-3.9 \pm 0.9$
$^{20}\text{Ne}$	-11.4	-12.4	-12.1	$-23 \pm 3$
$^{22}\text{Ne}$	-12.3	-12.3	-13.6	$-19 \pm 4$
$^{24}\text{Mg}$	-15.9	-16.3	-15.0	$-18 \pm 2$
$^{28}\text{Si}$	11.4	14.0	14.3	$16 \pm 3$
$^{30}\text{Si}$	-4.0	0.97	-6.6	$-5 \pm 6$
$^{32}\text{S}$	-11.9	-7.7	-13.6	$-15.4 \pm 2.0$
$^{34}\text{S}$	9.5	7.7	6.7	$4 \pm 3$
$^{36}\text{Ar}$	13.4	12.1	14.3	$11 \pm 6$
$^{42}\text{Ca}$	0.63	0.57	1.90	$-19 \pm 8$
$^{46}\text{Ti}$	-20.1	-21.9	-11.1	$-21 \pm 6$
$^{50}\text{Cr}$	-26.7	-30.0	-26.4	$-36 \pm 7$
$^{54}\text{Fe}$	-15.1	-17.9	-22.6	$-5 \pm 14$
$^{58}\text{Ni}$	-16.0	-16.2	-2.4	$-10 \pm 6$